Dual-Peak Absorbing Semiconducting Copolymer Nanoparticles for First and Second Near-Infrared Window Photothermal Therapy: A Comparative Study

Jiang, Yuyan; Li, Jingchao; Zhen, Xu; Xie, Chen; Pu, Kanyi

2018

Jiang, Y., Li, J., Zhen, X., Xie, C., & Pu, K. (2018). Dual-Peak Absorbing Semiconducting Copolymer Nanoparticles for First and Second Near-Infrared Window Photothermal Therapy: A Comparative Study. Advanced Materials, 30(14), 1705980-.

https://hdl.handle.net/10356/88821

https://doi.org/10.1002/adma.201705980

WILEY-VCH

DOI: 10.1002/adma.201705980
Article type: Communication

Dual-peak Absorbing Semiconducting Copolymer Nanoparticles for First and Second Near-Infrared Window Photothermal Therapy – A Comparative Study

*Yuyan Jiang, Jingchao Li, Xu Zhen, Chen Xie, and Kanyi Pu**

Y. Jiang, Dr J. Li, Dr X. Zhen, Dr C. Xie, Prof. K. Pu
School of Chemical and Biomedical Engineering
Nanyang Technological University
70 Nanyang Drive, 637457, Singapore
E-mail: kypu@ntu.edu.sg

Keywords: semiconducting polymer nanoparticles, photothermal therapy, second near-infrared window, cancer therapy

Abstract. Near-infrared (NIR) light is widely used for non-invasive optical diagnosis and phototherapy. However, current research focuses on the first NIR window (NIR-I, 650-950 nm), while the second NIR window (NIR-II, 1000-1700 nm) is far less exploited. Particularly, the practical advantages of NIR-II over NIR-I light for cancer photothermal therapy (PTT) remain to be revealed. We herein report the development of the first organic photothermal nanoagent (SPN_{I-II}) with dual-peak absorption in both NIR windows and its utilization in PTT. Such a nanoagent comprises a semiconducting copolymer with two distinct segments that respectively and identically absorb NIR light at 808 and 1064 nm. With the photothermal conversion efficiency of 43.4% at 1064 nm generally higher than other inorganic nanomaterials, SPN_{I-II} enables superior deep-tissue heating at 1064 nm over that at 808 nm at their respective safety limits. Model deep-tissue cancer PTT at a tissue depth of 5 mm validates the enhanced antitumor effect of SPN_{I-II} when shifting laser irradiation from NIR-I to NIR-II window. The good biodistirbubtion and facile synthesis of SPN_{I-II} also allow to dope it with a NIR dye for fluorescence imaging guided NIR-II PTT through systemic administration. Thus, our study paves the way for the development of new polymeric nanomaterials to advance phototherapy.

Near-infrared (NIR) light has been intensively exploited in biomedical applications due to its unrivaled benefits such as non-invasive manipulation, accurate remote control, and high tissue transparency.[1] Although most studies are focused on the first NIR (NIR-I) window (650-950 nm),[2] there is growing interest to extend the wavelength to the longer second NIR (NIR-II) window (1000-1700 nm).[3] Such light window has been recently identified to exhibit intrinsic advantages of deeper tissue penetration and higher maximum permissible exposure (MPE) as a respective result of reduced tissue scattering and lower energy of photons at longer wavelengths.[4] In contrast to NIR-I window, NIR-II light has been validated in vivo to afford enhanced spatial resolution and increased signal-to-background ratio for fluorescence and photoacoustic (PA) imaging, respectively.[4b, 5] Despite the progress of NIR-II light in imaging, few studies have been conducted to highlight its potential in deep-tissue photothermal therapy (PTT), mainly because nanomaterials that absorb NIR-II light are rare and limited to few inorganic systems such as gold nanostructures,[6] single-walled carbon nanotubes,[7] palladium nanoparticles,[8] bismuth nanoparticles,[9] copper selenide nanoparticles and ammonium-tungsten-bronze nanocubes.[10] In particular, the advantages of NIR-II relative to NIR-I window in terms of PTT remain experimentally unclear owning to the lack of adequate nanomaterials for a fair comparison.

The key challenge to develop photothermal agent for such a comparative study lies in the development of nanosystems with well-defined size and absorption in both NIR-I and NIR-II regions,[11] which requires precise control of bandgaps in a discrete way that is difficult for inorganic semiconductors.[12] As a new category of organic optical agents, semiconducting polymer nanoparticles (SPNs) are composed of π-conjugated polymer backbones, whose bandgaps are determined by the building-block monomers used for polymerization.[13] Due to the nature of benign organic components, SPNs circumvent the concern of metal-ion induced toxicity which is often encountered in inorganic materials,[14] and also possess size and morphology-independent optical properties.[15] Moreover, bandgap engineering provides a way to make SPNs with high photothermal conversion efficiency, allowing for efficient PTT and PA imaging.[16] Most SPN-based materials can only be responsive to visible or NIR-I light,[15b, 17] and few have been used for NIR-II fluorescence and photoacoustic imaging.[4b, 18] However, SPNs with efficient absorption in NIR-II window have not been adequately developed for cancer PTT, not to mention those with the absorption in both NIR-I and NIR-II windows.

We herein report the development of the first organic photothermal nanoagent with the dual-peak absorption in both NIR-I and NIR-II windows for cancer PTT. Such a nanoagent is

composed of a semiconducting copolymer, poly[(diketopyrrolopyrrole-*alt*-cyclopentadithiophene)-*ran*-(diketopyrrolopyrrole-*alt*-thiadiazoloquinoxaline)] (PDCDT), which has two different segments showing absorption in NIR-I and NIR-II windows, respectively. Finetuning of the ratio between two segments leads to a final polymer with the nearly identical absorbance at 808 and 1064 nm. The resulted SPN (SPN_{I-II}) not only allows for deep-tissue NIR-II PTT but also provides the opportunity to conduct a fair comparative study between NIR-I and NIR-II windows in order to reveal the superiority of NIR-II over NIR-I light for PTT. In the following, the design and synthesis of SPN_{I-II} are first described, followed by the characterization of its morphological, optical, and photothermal properties. Then, the deep-tissue photothermal heating capabilities of SPN_{I-II} are studied and compared for NIR-I and NIR-II light. The proof-of-concept application of SPN_{I-II} is demonstrated in tumor xenograft mouse model to validate the advantage of NIR-II window over NIR-I window for deep-tissue PTT. At last, a NIR dye (NIR775) is doped into SPN_{I-II} to afford a fluorescent nanoparticle ($SPNF_{I-II}$), permitting NIR fluorescence (NIRF) imaging guided NIR-II PTT is shown.

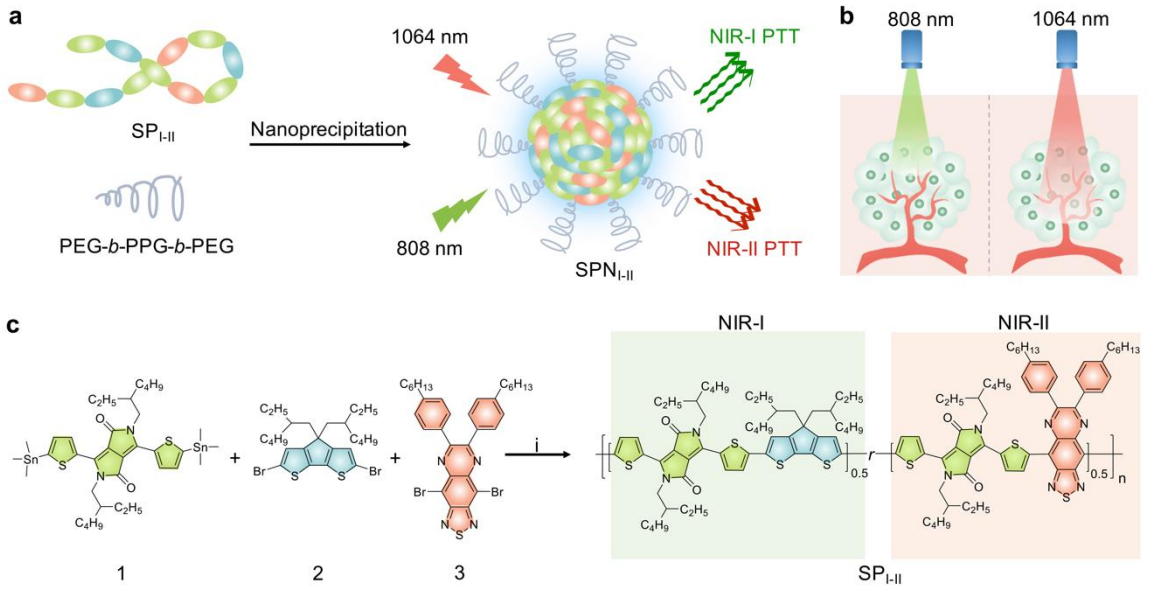

Figure 1. Design and synthesis of SPN_{I-II}. (a) Synthesis of SPN_{I-II} via nanoprecipitation. (b) Scheme that illustrates the deeper tissue penetration of 1064 nm relative to that of 808 nm. Power density: 808 nm, 0.3 W cm^{-2}; 1064 nm, 1 W cm^{-2}. (c) Synthetic route of SP_{I-II}. (i) $PdCl_2(PPh_3)_2$ and 2,6-di-*tert*-butylphenol, 100 ℃ for 4 h.

To obtain dual-NIR-window absorbing agents, a series of semiconducting copolymers based on PDCDT were synthesized via stille polycondensation of monomer 1, 2, and 3 (**Figure 1c**, **Table S1**, Supporting Information). Owning to the strong electron-withdrawing ability of thiadiazoloquinoxaline which further narrowed the bandgap and subsequently redshifted the absorption,[19] the absorbance of PDCDT at 1064 nm gradually increased concomitant with a drop of absorption at 808 nm when increasing the feed ratio of monomer 3 (**Figure S1a**, Supporting Information). At the molar ratio of 2:1:1 for monomer 1, 2, and 3, the polymer, $SP_{I\text{-}II}$, had the nearly identical absorbance at 1064 and 808 nm ($A_{1064}/A_{808} \approx 1$), and thus was used for the preparation of dual-NIR-window absorbing photothermal agent (**Figure 1c**, **Figure S1b**, Supporting Information).

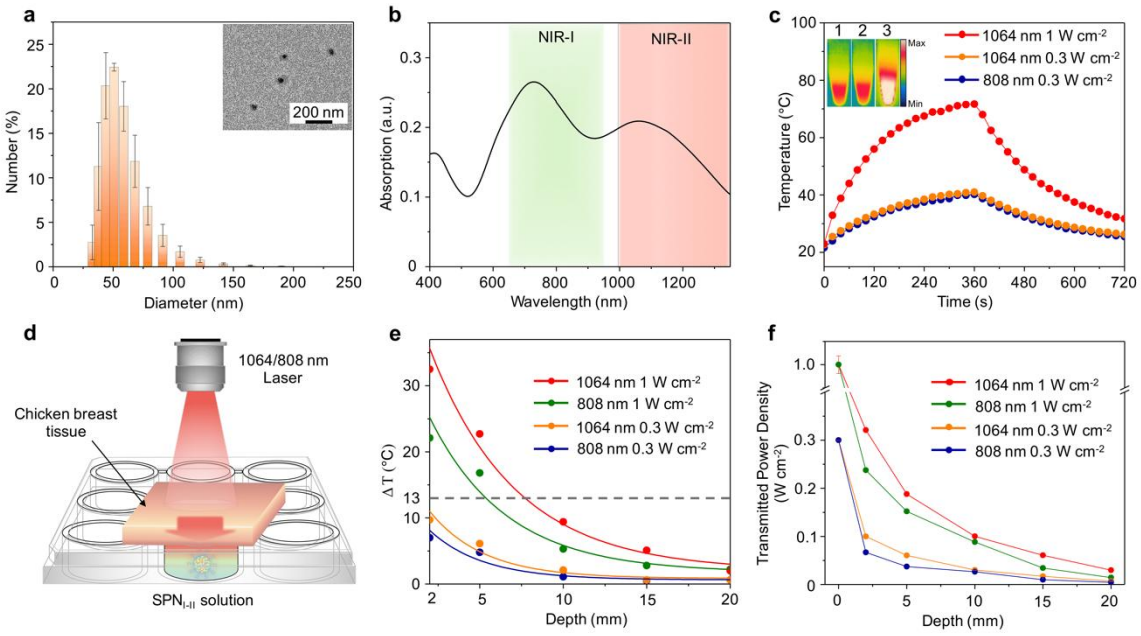

Figure 2. Characterization of $SPN_{I\text{-}II}$s. (a) DLS profile of $SPN_{I\text{-}II}$s in 1 × PBS. Error bars indicated standard deviations of three separate measurements. Inset: Representative TEM image of $SPN_{I\text{-}II}$s. (b) Vis-NIR absorption spectrum of $SPN_{I\text{-}II}$s in 1 × PBS (9 μg mL^{-1}). (c) Photothermal heating and cooling curves of $SPN_{I\text{-}II}$ solutions (20 μg mL^{-1}) under different laser conditions. Inset: IR thermal images of $SPN_{I\text{-}II}$ solutions at their representative maximum temperatures under different laser conditions. (1) 808 nm, 0.3 W cm^{-2}; (2) 1064 nm, 0.3 W cm^{-2}; (3) 1064 nm, 1 W cm^{-2}. (d) Schematic illustration of deep tissue photothermal study. (e) Fitted exponential decay of temperature change of $SPN_{I\text{-}II}$ solution (50 μg mL^{-1}) at different

depths of chicken breast tissue under different laser conditions. Grey line: Δ T = 13 ℃. (f) Transmitted power density of 1064 and 808 nm lasers at different depths of chicken breast tissue.

SP_{I-II} was subsequently transformed into water-soluble SPN_{I-II}s via nanoprecipitation with an amphiphilic tri-block copolymer PEG-*b*-PPG-*b*-PEG (**Figure 1a**). The uniform spherical morphology of SPN_{I-II} was indicated by transmission electron microscope (TEM) (**Figure 2a**), and the average hydrodynamic diameter of SPN_{I-II} was about 56 nm as revealed by dynamic light scattering (DLS) (Figure **2a**). The SPN_{I-II} solution was clear in turquoise and no precipitation or obvious change in diameter was observed after storage of SPN_{I-II} in 1 × PBS for two months (**Figure S3**, supporting information), suggesting their excellent aqueous stability. Optical properties of SPN_{I-II}s in 1 × PBS were studied. SPN_{I-II} had two absorption peaks at 728 and 1059 nm in the NIR-I and NIR-II windows, respectively (**Figure 2b**). The mass extinction coefficient of SPN_{I-II} at 808 nm was 25 $cm^{-1}mg^{-1}mL$, nearly identical to that at 1064 nm (23 $cm^{-1}mg^{-1}mL$). Cell viability assay verified the good cytocompatibility of SPN_{I-II} against 4T1 cells at a high concentration up to 200 μg mL^{-1} (**Figure S4**, Supporting Information).

Photothermal properties of SPN_{I-II}s were investigated and compared in both NIR-I and NIR-II windows. Under continuous laser irradiation at 808 nm or 1064 nm, the temperature of SPN_{I-II} solution gradually increased and reached a plateau at t = 360 s (**Figure 2c**). The maximum temperature of SPN_{I-II} solution irradiated at 808 nm at its MPE limit of 0.3 W cm^{-2} was 40.2 ℃, similar to that irradiated at 1064 nm at the same power density (41.0 ℃). Such comparable heating capabilities of SPN_{I-II} at both wavelengths should be attributed to the similar absorbance. In fact, the photothermal conversion efficiency of SPN_{I-II} at 808 nm (44.9%) was close to that at 1064 nm (43.4%) when measured at a power density of 0.3 W cm^{-2}.[20] Such an efficiency was higher than that of most photothermal agents reported in NIR-II window.[6a, 8-10]

When increasing the power density to the MPE limit for 1064 nm laser (1 W cm^{-2}), the maximum temperature of SPN_{I-II} solution irradiated at 1064 nm increased to 71.7 ℃, which was slightly higher than that irradiated at 808 nm (68.1 ℃). This small difference should be probably attributed to the heat contribution of water owning to its higher absorption at 1064 nm relative to that at 808 nm (**Figure S5**, Supporting Information). Note that the maximum temperature of SPN_{I-II} solution irradiated at 1064 nm laser was ~1.8-fold of that irradiated at 808 nm at their respective MPE limit. This fact highlights the practical superiority of the NIR-II window over the NIR-I window in photothermal heating. Moreover, the photothermal maximum temperature remained nearly the same after the reversible heating and cooling SPN_{I-II} solution irradiated at 1064 nm with the power of 1 W cm^{-2} (**Figure S6**, Supporting Information). Such an excellent photothermal stability of SPN_{I-II} was beneficial for in vivo applications.

To compare the deep-tissue photothermal heating capabilities between the NIR-I and NIR-II laser wavelengths, the SPN_{I-II} solution was filled in a 96-well plate covered by chicken breast tissue of various thicknesses (2, 5, 10, 15, and 20 mm) and then irradiated at 1064 or 808 nm at the power density of 0.3 or 1 W cm^{-2} for 10 min (**Figure 2d**, **Figure S7**, Supporting Information). The maximum temperature changes of SPN_{I-II} solution under these different conditions were summarized and plotted as a function of tissue depth and fitted by exponential decay curves (**Figure 2e**, **Table S2**, Supporting Information). When comparing at the same laser power density, the temperature change of SPN_{I-II} solution irradiated at 1064 nm was higher than that at 808 nm at each tissue depth. Such superiority should be attributed to the higher transmittance of 1064 nm laser relative to 808 nm laser as measured at each tissue depth at the same power density (**Figure 2f**). When comparing at their respective MPE limit for the practical purpose, the temperature change of SPN_{I-II} solution irradiated at 1064 nm was

4.6-, 4.7-, 8.5-, and 3.3-fold of that irradiated at 808 nm at tissue depths of 2, 5, 10, and 20 mm, respectively. All of these data emphasized the superior deep tissue photothermal heating capability under laser irradiation at 1064 nm over that at 808 nm. This should be ascribed to the intrinsically deeper tissue penetration in conjunction with the higher MPE limit of laser in the NIR-II window relative to that in the NIR-I window.[4] It should be noted that a temperature increase of 22.7 ºC was obtained with the maximum tissue depth of 5 mm under laser irradiation at 1064 nm with the power density of 1 W cm^{-2}. Considering the threshold temperature for PTT (43 ºC) and the average body temperature of living mice (~30 ºC during anesthesia),[21] such a temperature increment was well above the required temperature rise (13 ºC) and sufficient to ablate cancer cells in living mice.

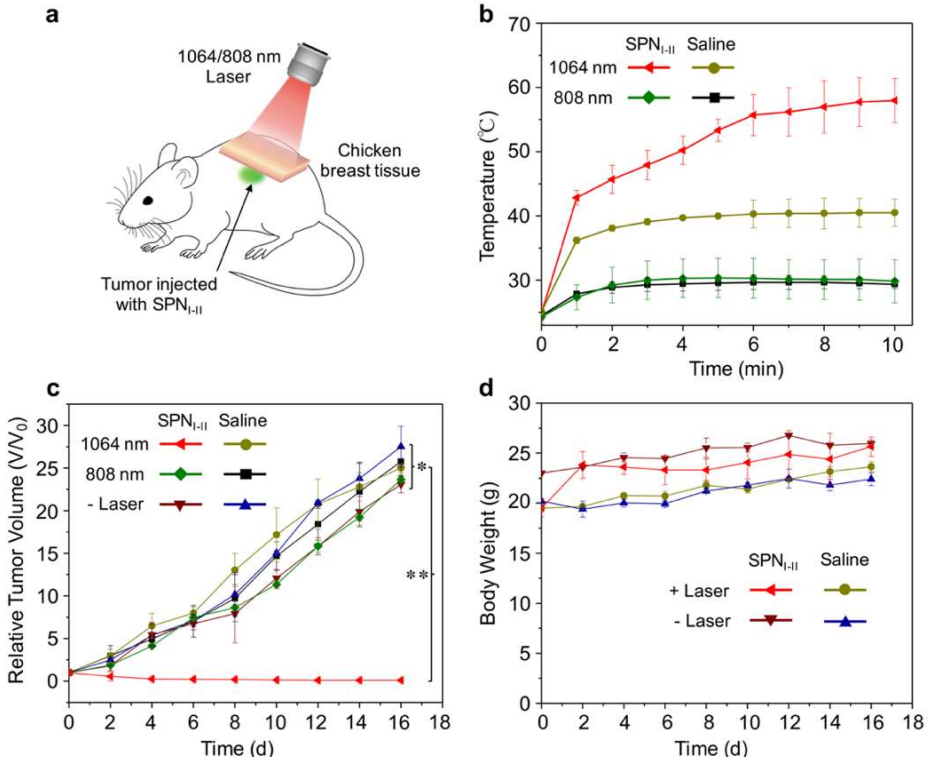

Figure 3. In vivo deep tissue PTT in NIR-I and NIR-II windows. (a) Schematic illustration of deep tissue PTT. Nude mice bearing xenograft 4T1 tumors on the left and right sides of the back were intratumorally injected with SPN_{I-II} (50 µL, 200 µg mL^{-1}) or saline (50 µL), respectively. A piece of 5 mm chicken breast tissue was placed on top of the tumor during laser irradiation. Power density: 1064 nm, 1 W cm^{-2}; 808 nm, 0.3 W cm^{-2}. (b) Mean tumor temperature as a function of laser irradiation time after intratumoral administration of SPN_{I-II}

(n=3). (c) Tumor growth curves and (d) body weight data of mice after intratumoral administration of SPN_{I-II} or saline with and without irradiation of 808 or 1064 nm laser (n = 3). (*p > 0.1, **p < 0.01) Error bars indicated standard error of mean (SEM) (n = 3).

To validate the advantage of the NIR-II window over the NIR-I window for in vivo deep-tissue PTT, SPN_{I-II} was intratumorally injected into the nude mice bearing 4T1 xenograft tumor and then laser irradiation was conducted in the presence of a piece of 5 mm chicken breast tissue placed on the top of the tumor to mimic the deep tissue environment. To further align such experiments with the practical conditions, laser irradiation at 808 or 1064 nm was conducted at their respective MPE (1 W cm^{-2} for 1064 nm and 0.3 W cm^{-2} for 808 nm) (**Figure 3a**). As shown in **Figure 3b**, at each time point, the temperature of SPN_{I-II}-injected tumor irradiated at 1064 nm was higher than that irradiated at 808 nm. After laser irradiation for 10 min, the temperature of SPN_{I-II}-injected tumor irradiated at 1064 nm was 58.0 ℃, which was 1.9- and 1.4-fold of that for SPN_{I-II}-injected tumor irradiated at 808 nm (29.8 ℃) and saline-treated tumor irradiated at 1064 nm (40.5 ℃), respectively. Noteworthy that laser irradiation at 808 nm with its MPE did not bring the tumor temperature above the threshold PTT temperature required to induce apoptosis (43 ℃). These data confirmed that laser irradiation at 1064 nm was superior over that at 808 nm for deep-tissue heating, which was consistent with the in vitro results (**Figure 2f**).

To evaluate the deep tissue photothermal antitumor efficacy for both NIR-I and NIR-II lasers, the volumes of tumors in living mice were continuously measured for 16 days after photothermal treatment (**Figure 3c**). Note that no significant weight loss of mice was observed for all groups (**Figure 3d**), indicating the safety of all treatments. The tumors injected with SPN_{I-II} were totally ablated after irradiation of 1064 nm laser at 1 W cm^{-2} and the tumor growth was successfully inhibited throughout the experimental period. In contrast, the tumor injected with SPN_{I-II} irradiated at 808 nm laser at 0.3 W cm^{-2} grew nearly as fast as

those treated with saline with or without laser irradiation. Thus, PTT in the NIR-II window afforded superior deep-tissue antitumor efficacy over that in the NIR-I window, which should be attributed to the combination of higher MPE and intrinsically deeper tissue penetration for that in the NIR-II window.

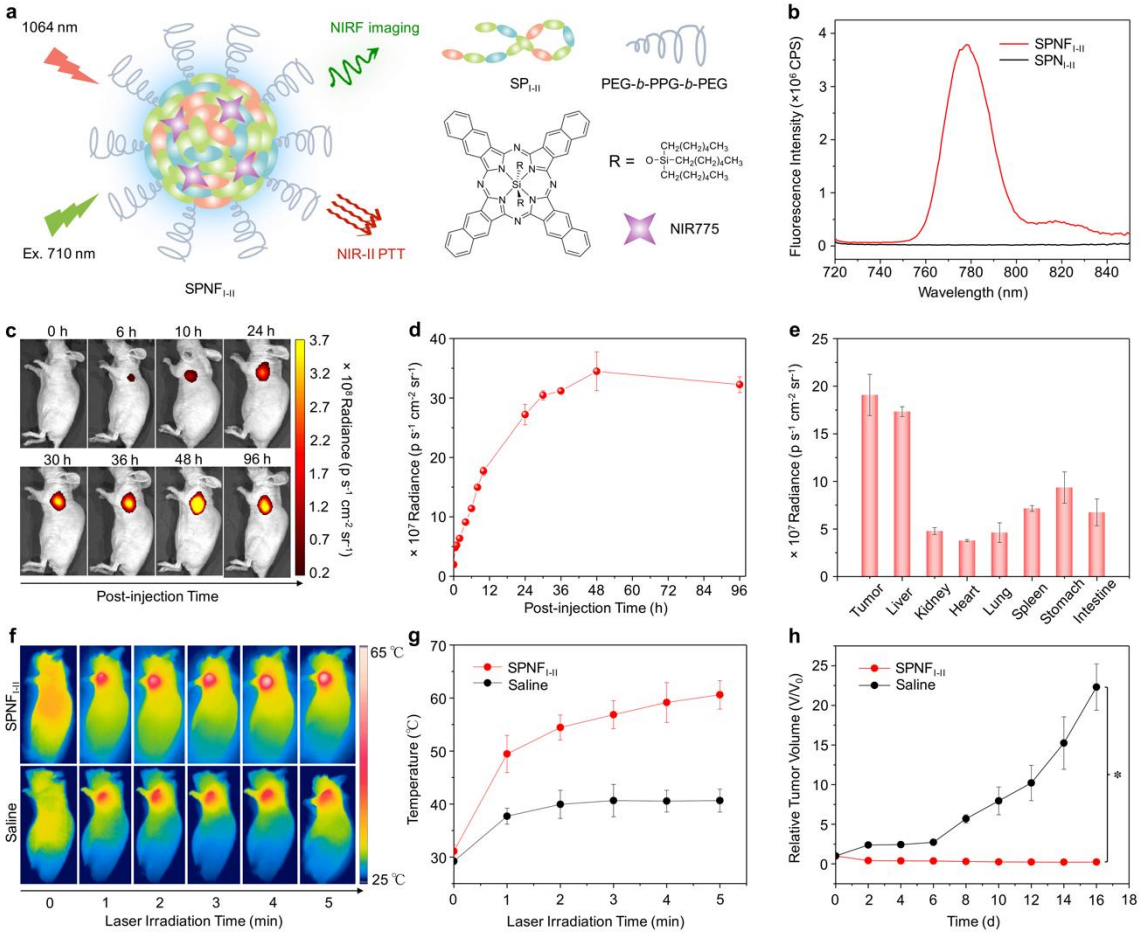

Figure 4. In vivo NIRF imaging and NIR-II PTT. (a) Schematic illustration of $SPNF_{I\text{-}II}$. (b) Fluorescence spectra of $SPN_{I\text{-}II}$ and $SPNF_{I\text{-}II}$ in 1 × PBS ($SP_{I\text{-}II}$, 10 μg mL^{-1}). Excitation wavelength: 710 nm. (c) Fluorescence images of living mice bearing xenograft 4T1 tumors at 0, 6, 10, 24, 30, 36, 48, and 96 h after systemic administration of $SPNF_{I\text{-}II}$ through tail-vein injection (200 μL, $SP_{I\text{-}II}$ 200 μg mL^{-1}). All the fluorescence data were collected with excitation and emission at 710 and 780 nm, respectively. (d) Fluorescence intensity extracted from tumor regions as a function of time after administration of $SPNF_{I\text{-}II}$ (n = 3). (e) Ex vivo quantification of average fluorescence intensity of tumors and major organs of mice at 96 h after systemic administration of $SPNF_{I\text{-}II}$ (n = 3). (f) IR thermal images of 4T1 tumor-bearing mice under irradiation of 1064 nm laser (1 W cm^{-2}) at 48 h after systemic administration of

$SPNF_{I-II}$ (200 μL, SP_{I-II} 200 μg mL^{-1}) or saline (200 μL). (g) Mean tumor temperature as a function of laser irradiation time at 48 h after systemic administration of $SPNF_{I-II}$ (200 μL, SP_{I-II} 200 μg mL^{-1}) or saline (200 μL) (n = 3). (h) Tumor growth curves of mice after intravenous administration of $SPNF_{I-II}$ (200 μL, SP_{I-II} 200 μg mL^{-1}) or saline (200 μL) with laser treatment (n = 3). (*$p < 0.01$) Error bars indicated standard error of mean (SEM) (n = 3).

The efficacy for the NIR-II PPT was further tested after systemic administration of SPN. To identify the optimal therapeutic window, nanoparticles were doped with a NIR dye, silicon 2,3-naphthalocyanine bis(trihexylsilyloxide) (NIR775), at a weight ratio of 2%, so that NIR fluorescence imaging could be conducted to monitor the accumulation of nanoparticles in tumor (**Figure 4a**, **Figure S8a & b**, Supporting Information). The size and morphology of the as-prepared $SPNF_{I-II}$ remained almost the same with SPN_{I-II} before doping (**Figure S8c & d**, Supporting Information). Different from no fluorescent SPN_{I-II}, $SPNF_{I-II}$ was fluorescent with the emission maximum at 778 nm (**Figure 4b**). After systemic administration of $SPNF_{I-II}$ into 4T1-bearing nude mice via tail-vein injection, the fluorescence images were longitudinally recorded and quantified (**Figures 4c & d**). The fluorescence intensity in the tumor region gradually increased, and reached the maximum at 48 h post-injection of $SPNF_{I-II}$, which was ~17.5-fold of the background. This indicated that $SPNF_{I-II}$ could passively target tumors through enhanced permeability and retention (EPR) effect, probably due to their small size (54 nm) and PEG-coated surfaces.[22] Ex vivo biodistribution data further validated that the tumor had the strongest fluorescence intensity, followed by liver, stomach, spleen, and other organs (**Figure 4e**, **Figure S9**, Supporting Information).

According to the NIR fluorescence (NIRF) imaging (**Figure 4d**), PTT in the NIR-II window was conducted at the optimal therapeutic window (48 h) after systemic administration of $SPNF_{I-II}$ or saline via tail vein injection. Upon irradiation of 1064 nm laser at 1 W cm^{-2}, the temperature of tumor region for $SPNF_{I-II}$ treated mice gradually increased (**Figure 4f and g**), which was significantly higher than that for saline-treated groups at all

time points. After laser irradiation for 5 min, the average temperature of tumor on $SPNF_{I-II}$ treated mice reached 61 ℃, 1.5-fold of that for saline-treated groups (40 ℃). To quantitatively evaluate the antitumor effect for the NIR-II PTT using $SPNF_{I-II}$, tumor sizes were continuously measured for 16 days (**Figure 4h**). In contrast to the fast growth of tumors for saline-treated mice, the growth of tumors for $SPNF_{I-II}$ treated mice were successfully inhibited after PTT. Moreover, no obvious weight loss of mice was observed (**Figure S10**, Supporting Information) throughout experimental period. These data indicated the high therapeutic efficacy of NIR-II PTT using $SPNF_{I-II}$ along with the good biosafety.

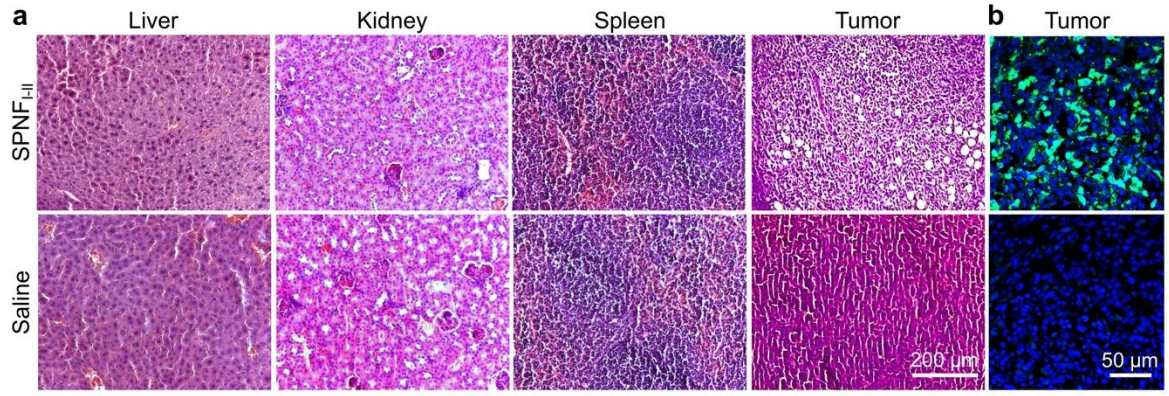

Figure 5. Histological analysis. (a) H&E staining for livers, kidneys, spleens, and tumors of mice treated with $SPNF_{I-II}$ or saline after NIR-II photothermal treatment. (b) Immunofluorescent staining of caspase-3 for tumors on mice treated with $SPNF_{I-II}$ or saline after NIR-II photothermal treatment. Green fluorescence indicated staining of caspase-3, while blue fluorescence indicated nucleus staining.

To further verify the therapeutic outcome of NIR-II light using $SPNF_{I-II}$, all the mice were sacrificed after NIR-II PTT. Hematoxylin and eosin (H&E) staining and immunofluorescent staining of caspase-3 were subsequently performed on tumors and different organs for histological analysis at day 2 after PTT. As shown in **Figure 5a**, no noticeable histopathological damage could be observed in livers, kidneys, and spleens of both $SPNF_{I-II}$- and saline-treated mice after NIR-II PTT. In comparison, typical nucleus dissociation was clearly observed for tumor tissues of $SPNF_{I-II}$-treated mice after PTT, suggesting the necrosis

and apoptosis of cancer cells triggered by PTT.[23] Additionally, the immunofluorescent staining of caspase-3 indicated the obvious apoptosis of cancer cells for $SPNF_{I-II}$-treated mice after PTT as witnessed by the strong green fluorescence in tumor tissue (**Figure 5b**). However, no noticeable apoptosis could be observed for saline-treated mice after laser irradiation (**Figure 5b**). These histological data validated at cellular level that the $SPNF_{I-II}$-mediated NIR-II PTT had a high antitumor efficacy, which was in agreement with in vivo results.

In conclusion, we have developed an organic photothermal nanoagent (SPN_{I-II}) that had dual-peak absorption in both NIR-I and NIR-II windows. Such a unique spectral profile was achieved by incorporation of three structure units with different electron–withdrawing or –donating ability into a single semiconducting copolymer (SP_{I-II}), followed by its formulation into water-soluble nanoparticles. SPN_{I-II} had the photothermal conversion efficiencies of 44.9 and 43.4% at 808 and 1064 nm, respectively, which were higher than most NIR-II absorbing nanomaterials. With the nearly identical absorbance at 1064 and 808 nm, SPN_{I-II} was utilized for the comparison of deep-tissue photothermal heating capabilities between NIR-I and NIR-II light. The results revealed that at their respective MPE, the photothermal maximum temperature of SPN_{I-II} irradiated at 1064 nm was 4.6-, 4.7-, 8.5-, and 3.3-fold of that irradiated at 808 nm at tissue depths of 2, 5, 10, and 20 mm, respectively. Such a deep-tissue heating superiority of NIR-II relative to NIR-I light eventually led to better antitumor efficacy for NIR-II PTT in living mice. The facile synthesis of organic photothermal nanoagent allowed to dope with a NIR dye, resulting in a fluorescent nanoparticle ($SPNF_{I-II}$) for NIRF imaging guided NIR-II PTT through systemic administration. Both in vivo and ex vivo data confirmed that $SPNF_{I-II}$ passively targeted the tumor and effectively ablate cancer cells under NIR-II light irradiation while causing no damage to normal tissues in living mice. These data suggested that SPN_{I-II} had great potential for phototherapy in NIR-II window.

To the best of our knowledge, our study not only represents the first organic photothermal nanoagent having peak absorptions in both NIR-I and NIR-II region but also reveals the

importance of red-shifting the laser light from NIR-I into NIR-II window for deep-tissue PTT. Moreover, our SPN-based photothermal nanoagent can serve as a platform to integrate other functionalities such as imaging, immunotherapy, and chemotherapy, bringing in multimodality theranostics.[24]

Supporting Information

Supporting Information is available from the Wiley Online Library or from the author.

Acknowledgements

K.P. thanks Nanyang Technological University (Start-Up grant: NTU-SUG: M4081627.120) and Singapore Ministry of Education (Academic Research Fund Tier 1: RG133/15 M4011559 and Academic Research Fund Tier 2 MOE2016-T2-1-098) for the financial support.

References

[1] S.-m. Park, A. Aalipour, O. Vermesh, J. H. Yu, S. S. Gambhir, *Nat. Rev. Mater.* **2017**, *2*, 17014.

[2] a) V. Ntziachristos, D. Razansky, *Chem. Rev.* **2010**, *110*, 2783; b) J. Wang, F. Chen, S. J. Arconada-Alvarez, J. Hartanto, L.-P. Yap, R. Park, F. Wang, I. Vorobyova, G. Dagliyan, P. S. Conti, J. V. Jokerst, *Nano Lett.* **2016**, *16*, 6265; c) J. Weber, P. C. Beard, S. E. Bohndiek, *Nat. Methods* **2016**, *13*, 639.

[3] a) G. Hong, A. L. Antaris, H. Dai, *Nat. Biomed. Eng.* **2017**, *1*, 0010; b) A. M. Smith, M. C. Mancini, S. Nie, *Nat. Nanotechnol.* **2009**, *4*, 710.

[4] a) Y. Cao, J.-H. Dou, N.-j. Zhao, S. Zhang, Y.-Q. Zheng, J.-P. Zhang, J.-Y. Wang, J. Pei, Y. Wang, *Chem. Mater.* **2017**, *29*, 718; b) Y. Jiang, P. K. Upputuri, C. Xie, Y. Lyu, L. Zhang, Q. Xiong, M. Pramanik, K. Pu, *Nano Lett.* **2017**, *17*, 4964.

[5] a) G. Ku, M. Zhou, S. Song, Q. Huang, J. Hazle, C. Li, *ACS Nano* **2012**, *6*, 7489; b) Y. Zhou, D. Wang, Y. Zhang, U. Chitgupi, J. Geng, Y. Wang, Y. Zhang, T. R. Cook, J. Xia, J. F. Lovell, *Theranostics* **2016**, *6*, 688.

[6] a) X. Ding, C. H. Liow, M. Zhang, R. Huang, C. Li, H. Shen, M. Liu, Y. Zou, N. Gao, Z. Zhang, Y. Li, Q. Wang, S. Li, J. Jiang, *J. Am. Chem. Soc.* **2014**, *136*, 15684; b) M.-F. Tsai, S.-H. G. Chang, F.-Y. Cheng, V. Shanmugam, Y.-S. Cheng, C.-H. Su, C.-S. Yeh, *ACS Nano* **2013**, *7*, 5330; c) P. Vijayaraghavan, C.-H. Liu, R. Vankayala, C.-S. Chiang, K. C. Hwang, *Adv. Mater.* **2014**, *26*, 6689.

[7] A. L. Antaris, J. T. Robinson, O. K. Yaghi, G. Hong, S. Diao, R. Luong, H. Dai, *ACS Nano* **2013**, *7*, 3644.

[8] M. Manikandan, N. Hasan, H.-F. Wu, *Biomaterials* **2013**, *34*, 5833.

[9] a) A. Li, X. Li, X. Yu, W. Li, R. Zhao, X. An, D. Cui, X. Chen, W. Li, *Biomaterials* **2017**, *112*, 164; b) X. Yu, A. Li, C. Zhao, K. Yang, X. Chen, W. Li, *ACS Nano* **2017**, *11*, 3990.

[10] a) C. Guo, H. Yu, B. Feng, W. Gao, M. Yan, Z. Zhang, Y. Li, S. Liu, *Biomaterials* **2015**, *52*, 407; b) Z.-C. Wu, W.-P. Li, C.-H. Luo, C.-H. Su, C.-S. Yeh, *Adv. Funct. Mater.* **2015**, *25*, 6527.
[11] L. Cheng, C. Wang, L. Feng, K. Yang, Z. Liu, *Chem. Rev.* **2014**, *114*, 10869.
[12] Y. Dai, C. Xu, X. Sun, X. Chen, *Chem. Soc. Rev.* **2017**, *46*, 3830.
[13] a) K. Pu, A. J. Shuhendler, J. V. Jokerst, J. Mei, S. S. Gambhir, Z. Bao, J. Rao, *Nat. Nanotechnol.* **2014**, *9*, 233; b) K. Pu, J. Mei, J. V. Jokerst, G. Hong, A. L. Antaris, N. Chattopadhyay, A. J. Shuhendler, T. Kurosawa, Y. Zhou, S. S. Gambhir, *Adv. Mater.* **2015**, *27*, 5184.
[14] K. Pu, N. Chattopadhyay, J. Rao, *J. Control. Release* **2016**, *240*, 312.
[15] a) L. Feng, C. Zhu, H. Yuan, L. Liu, F. Lv, S. Wang, *Chem. Soc. Rev.* **2013**, *42*, 6620; b) J. Yu, Y. Rong, C.-T. Kuo, X.-H. Zhou, D. T. Chiu, *Anal. Chem.* **2017**, *89*, 42.
[16] a) Y. Jiang, D. Cui, Y. Fang, X. Zhen, P. K. Upputuri, M. Pramanik, D. Ding, K. Pu, *Biomaterials* **2017**, *145*, 168; b) Y. Jiang, K. Pu, *Small* **2017**, 1700710; c) Y. Lyu, Y. Fang, Q. Miao, X. Zhen, D. Ding, K. Pu, *ACS Nano* **2016**, *10*, 4472; d) Y. Lyu, X. Zhen, Y. Miao, K. Pu, *ACS Nano* **2016**, *11*, 358; e) Q. Miao, Y. Lyu, D. Ding, K. Pu, *Adv. Mater.* **2016**, *28*, 3662; f) C. Yin, X. Zhen, Q. Fan, W. Huang, K. Pu, *ACS Nano* **2017**, *11*, 4174; g) J. Zhang, X. Zhen, P. K. Upputuri, M. Pramanik, P. Chen, K. Pu, *Adv. Mater.* **2016**, *27*, 1604764.
[17] a) X. Wang, S. Li, P. Zhang, F. Lv, L. Liu, L. Li, S. Wang, *Adv. Mater.* **2015**, *27*, 6040; b) I. C. Wu, J. Yu, F. Ye, Y. Rong, M. E. Gallina, B. S. Fujimoto, Y. Zhang, Y.-H. Chan, W. Sun, X.-H. Zhou, C. Wu, D. T. Chiu, *J. Am. Chem. Soc.* **2015**, *137*, 173; c) C.-T. Kuo, A. M. Thompson, M. E. Gallina, F. Ye, E. S. Johnson, W. Sun, M. Zhao, J. Yu, I. C. Wu, B. Fujimoto, C. C. DuFort, M. A. Carlson, S. R. Hingorani, A. L. Paguirigan, J. P. Radich, D. T. Chiu, *Nat. Commun.* **2016**, *7*, 11468; d) K. Sun, Y. Tang, Q. Li, S. Yin, W. Qin, J. Yu, D. T. Chiu, Y. Liu, Z. Yuan, X. Zhang, C. Wu, *ACS Nano* **2016**, *10*, 6769; e) H.-Y. Liu, P.-J. Wu, S.-Y. Kuo, C.-P. Chen, E.-H. Chang, C.-Y. Wu, Y.-H. Chan, *J. Am. Chem. Soc.* **2015**, *137*, 10420; f) C.-S. Ke, C.-C. Fang, J.-Y. Yan, P.-J. Tseng, J. R. Pyle, C.-P. Chen, S.-Y. Lin, J. Chen, X. Zhang, Y.-H. Chan, *ACS Nano* **2017**, *11*, 3166; g) A. J. Shuhendler, K. Pu, L. Cui, J. P. Uetrecht, J. Rao, *Nat. Biotechnol.* **2014**, *32*, 373; h) Y. Lyu, C. Xie, S. A. Chechetka, E. Miyako, K. Pu, *J. Am. Chem. Soc.* **2016**, *138*, 9049; i) Y. Lyu, D. Cui, H. Sun, Y. Miao, H. Duan, K. Pu, *Angew. Chem. Int. Edit.* **2017**, *129*, 9283; j) X. Zhen, Y. Tao, Z. An, P. Chen, C. Xu, R. Chen, W. Huang, K. Pu, *Adv. Mater.* **2017**, *29*, 1606665; k) H. Zhu, Y. Fang, Q. Miao, X. Qi, D. Ding, P. Chen, K. Pu, *ACS Nano* **2017**, *11*, 8998.
[18] a) S. Zhu, Q. Yang, A. L. Antaris, J. Yue, Z. Ma, H. Wang, W. Huang, H. Wan, J. Wang, S. Diao, B. Zhang, X. Li, Y. Zhong, K. Yu, G. Hong, J. Luo, Y. Liang, H. Dai, *Proc. Natl. Acad. Sci. USA* **2017**, 201617990; b) K. Shou, C. Qu, Y. Sun, H. Chen, S. Chen, L. Zhang, H. Xu, X. Hong, A. Yu, Z. Cheng, *Adv. Funct. Mater.* **2017**; c) Q. Yang, Z. Ma, H. Wang, B. Zhou, S. Zhu, Y. Zhong, J. Wang, H. Wan, A. Antaris, R. Ma, X. Zhang, J. Yang, X. Zhang, H. Sun, W. Liu, Y. Liang, H. Dai, *Adv. Mater.* **2017**, *29*; d) A. L. Antaris, H. Chen, K. Cheng, Y. Sun, G. Hong, C. Qu, S. Diao, Z. Deng, X. Hu, B. Zhang, X. Zhang, O. K. Yaghi, Z. R. Alamparambil, X. Hong, Z. Cheng, H. Dai, *Nat. Mater.* **2016**, *15*, 235; e) G. Hong, Y. Zou, A. L. Antaris, S. Diao, D. Wu, K. Cheng, X. Zhang, C. Chen, B. Liu, Y. He, J. Z. Wu, J. Yuan, B. Zhang, Z. Tao, C. Fukunaga, H. Dai, *Nat. Commun.* **2014**, *5*, 4206.
[19] T. T. Steckler, P. Henriksson, S. Mollinger, A. Lundin, A. Salleo, M. R. Andersson, *J. Am. Chem. Soc.* **2014**, *136*, 1190.
[20] C. M. Hessel, V. P. Pattani, M. Rasch, M. G. Panthani, B. Koo, J. W. Tunnell, B. A. Korgel, *Nano Lett.* **2011**, *11*, 2560.

[21] B. Hildebrandt, P. Wust, O. Ahlers, A. Dieing, G. Sreenivasa, T. Kerner, R. Felix, H. Riess, *Crit. Rev. Oncol./Hematol.* **2002**, *43*, 33.
[22] J. V. Jokerst, T. Lobovkina, R. N. Zare, S. S. Gambhir, *Nanomedicine* **2011**, *6*, 715.
[23] J. R. Melamed, R. S. Edelstein, E. S. Day, *ACS Nano* **2015**, *9*, 6.
[24] Q. Chen, L. Xu, C. Liang, C. Wang, R. Peng, Z. Liu, *Nat. Commun.* **2016**, *7*, 13193.

TOC

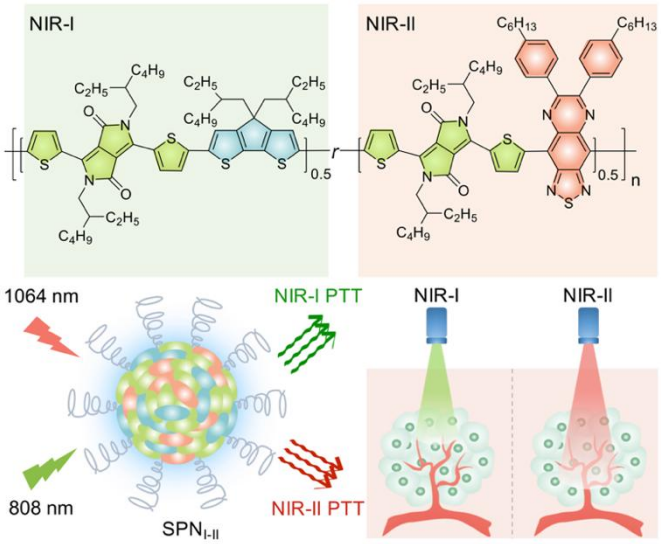

The first dual-peak absorbing organic nanoagent with nearly identical absorbance at 808 and 1065 nm is developed from a semiconducting copolymer. Such a nanoagent not only enables deep-tissue photothermal cancer therapy in both first and second near-infrared windows, but also permits a fair comparative study to reveal the advantage of shifting the laser light into longer wavelength region for phototherapy.